Two-phonon Raman scattering in graphene for laser excitation beyond the π-plasmon energy

2016 J. Phys.: Conf. Ser. 764 012008

(http://iopscience.iop.org/1742-6596/764/1/012008)

Journal of Physics: Conference Series **764** (2016) 012008 doi:10.1088/1742-6596/764/1/012008

Two-phonon Raman scattering in graphene for laser excitation beyond the π-plasmon energy

Valentin N Popov

Faculty of Physics, University of Sofia, BG-1164 Sofia, Bulgaria

E-mail: vpopov@phys.uni-sofia.bg

Abstract. The study of the two-phonon Raman spectra of graphene allows obtaining valuable information about the phonon dispersion inside the Brillouin zone. Up to now, the two-phonon Raman spectra have been extensively measured and modelled for laser excitation mainly in the visible range. However, recently, Raman measurements have been reported for laser excitation in the near ultraviolet range, close to the π-plasmon energy of about 5 eV. Here, we calculate the two-phonon Raman spectra in the latter range and compare the obtained results to the available Raman data. The crossover behaviour of the scattering of electrons by phonons on passing the π-plasmon energy is also discussed.

1. Introduction

Graphene has a two-dimensional honeycomb structure entirely consisting of carbon atoms [1] (figure 1). Its unique mechanical, optical, and electronic properties [2,3] make it suitable for application for thin transparent conducting electrodes, and flexible electronics and photonics [4]. Among the various experimental techniques, which are currently applied for the characterization of graphene samples, the Raman spectroscopy has become most popular because of its obvious advantages as an inexpensive and non-destructive method [5].

Graphene has a single Raman-active phonon, which gives rise to the so-called G band in the Raman spectra. A few peaks are normally observed in the second-order Raman spectra of graphene. In perfect graphene, the spectra are dominated by the so-called 2D band, which is several times more intense than the G band. It arises from scattering of electrons by phonons close to the K point in the Brillouin zone (figure 2). A few other two-phonon bands are also usually seen in the spectra. In the presence of defects, defect-induced Raman bands, which come from scattering by a defect and a phonon in the vicinity of the K point, are often detected. The two-phonon bands contain valuable information about the phonon dispersion, the electron-phonon and electron-photon couplings, doping, and strain in perfect graphene [6]. The G band and the second-order Raman bands originate from *resonant Raman scattering*, which has been attributed to the unique electronic band structure of graphene, consisting of bands with linear dispersion at the Fermi energy [7].

While the modelling of defect-induced bands relies on the unknown defect type and distribution, and significant advance in their quantitative description has not been achieved so far, there have been a number of reports on progress in the computation of the two-phonon bands for laser excitation in the visible range, predicting realistic position, lineshape, and dispersion rate of these bands [8,9].

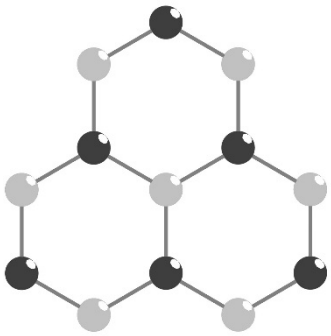

Figure 1. The atomic structure of graphene. The atoms of the two interpenetrating hexagonal lattices are drawn by light and dark grey circles.

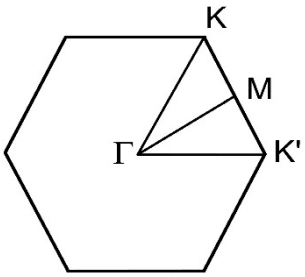

Figure 2. The hexagonal Brillouin zone of graphene with indicated special points.

Here, we extend the calculations of the two-phonon bands of Ref. [9] to laser excitation above the optical range and even beyond the π-plasmon energy of graphene, prompted by recent measurements of the Raman bands in this energy range [10]. We limit our report to two-phonon bands of in-plane optical phonons of graphene, which yield most intense Raman peaks. The paper is organized as follows. First, the underlying theory of the electron and phonon dispersions, as well as the resonant Raman intensity, is briefly dwelt on in Sec. 2. The obtained results for the overtone and combination bands are presented and discussed in Sec. 3. The paper ends up with conclusions.

2. Theoretical part

The resonant enhancement of the two-phonon Raman bands is a result of matching the incident photon energy with quantum transitions of the studied system. Therefore, the consistent modelling of the Raman bands requires quantum-mechanical description of the system of electrons, photons, phonons, and their interactions. Here, the calculation of the electronic band structure, phonon dispersion, and Raman intensity is performed within a density-functional-based non-orthogonal tight-binding model (NTB model) [11]. The NTB model uses Hamiltonian and overlap matrix elements with radial dependence derived from an *ab-initio* study on carbon dimers [12]. Only matrix elements between the four atomic orbitals of type s, p_x, p_y, p_z for the valence electrons of the carbon atoms are considered. The angular dependence of the matrix elements is described within the Slater – Koster scheme. The NTB model allows for the calculation of the total energy of the atomic structure with important application to the relaxation of the atomic structure, which is a necessary step before performing calculations of the phonon dispersion.

The phonon dispersion is derived using a perturbative approach within the NTB model [13]. The expression for the dynamical matrix makes use of the electron-phonon matrix elements, which are also derived within the NTB model [14].

Finally, the Raman intensity of a two-phonon Raman band can be calculated by means of the expression, obtained in fourth-order perturbation theory within the NTB model [9],

$$I \propto \sum_f \left| \sum_{c,b,a} \frac{M_{fc} M_{cb} M_{ba} M_{ai}}{\Delta E_{ic} \Delta E_{ib} \Delta E_{ia}} \right|^2 \delta\left(E_i - E_f\right). \quad (1)$$

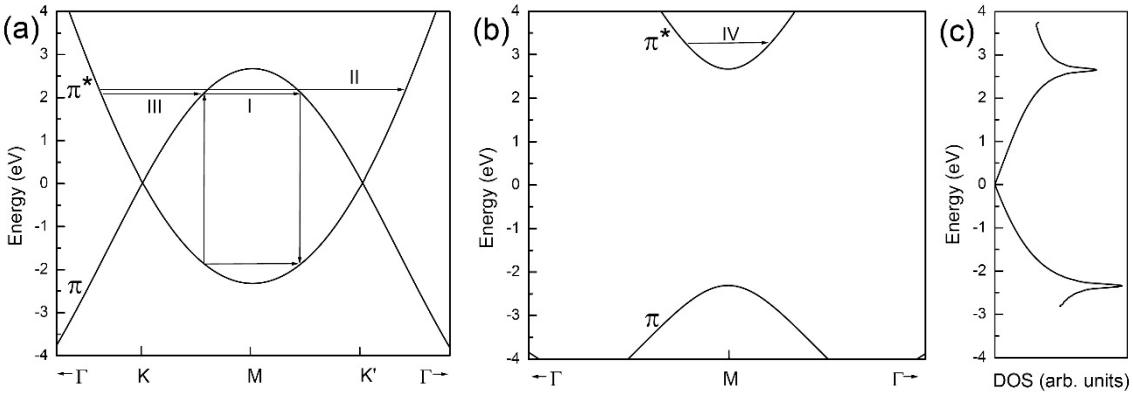

Figure 3. Electronic band structure of graphene along the high-symmetry directions: (a) ΓKMK′Γ and (b) ΓMΓ. Only the conduction π* band and valence π band close to the Fermi energy, taken to be zero, are shown. These bands have linear dispersion in the vicinity of the Fermi energy but have inflexion points at the M point. The electronic DOS, shown in panel (c), has logarithmic singularities at the inflexion points. For explanation of the notation, see text.

Here, $\Delta E_{iu} = E_i - E_u - i\gamma$, where E_u ($u = a,b,c$) are the energies of the intermediate states of the system of photons, electrons, holes, and phonons; E_i is the initial state energy, equal to the laser excitation energy E_L; γ is the sum of the halfwidths of pairs of electron and hole states, belonging to an intermediate system state, and will be referred to as the *electronic linewidth*; the approximation of wavevector-independent but energy-dependent electronic linewidth is adopted throughout the paper; M_{ai} and M_{fc} are the momentum matrix elements for creation and recombination of an electron-hole pair, respectively; M_{ba} and M_{cb} are the electron-phonon matrix elements for scattering between intermediate states. The electron-photon and electron-phonon matrix elements are calculated explicitly within the NTB model [14]. The summation over the intermediate states runs over all valence and conduction bands, and over all electron wavevectors **k**. The summation over the final states runs over the considered pair of phonon branches and over all phonon wavevectors **q**. For both summations, convergence is reached with a 400 × 400 mesh of **k** and **q** points in the Brillouin zone. The calculations are limited to in-plane parallel scattering configuration, backscattering geometry, and Stokes processes.

As it is seen from equation (1), the Raman intensity is resonantly enhanced, whenever in the sum there are terms, for which the real part of one, two, or three of the quantities ΔE_{iu} vanishes, i.e., the laser excitation matches well intermediate states of the system or, roughly speaking, matches the difference of the energies of the created electron and hole. Additionally, the Raman bands will be observable if the matrix elements in equation (1) are sufficiently large. On the contrary, terms, for which none of the energy denominators ΔE_{iu} is small, will give negligible contribution to the intensity, even if the matrix elements are not small.

3. Results and discussion

The honeycomb atomic structure of graphene has a unit cell of two atoms and can be considered as consisting of two interpenetrating hexagonal Bravais lattices (figure 1). Graphene has a hexagonal Brillouin zone with several characteristic special points (figure 2), among which the points Γ, M, K, and K′ are most important for this study as it will become clear below.

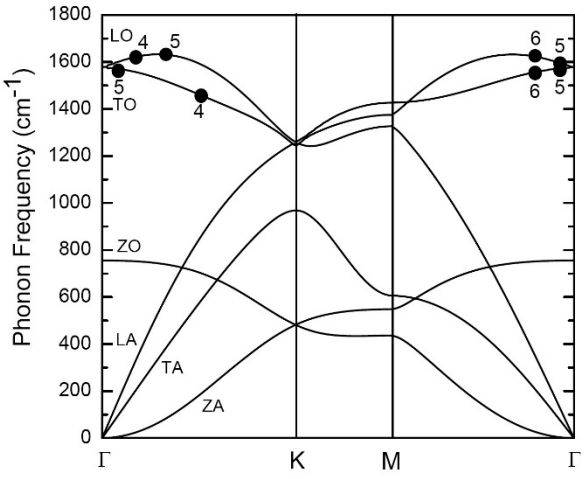

Figure 4. Phonon dispersion of graphene with displacement pattern for the branches. The circles mark the phonon wavevectors for two-phonon scattering at laser excitation, given by the numbers next to the symbols. For explanation of the branch notation, see text.

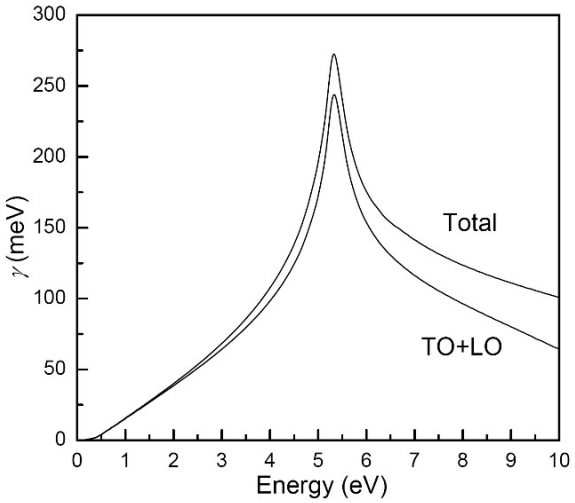

Figure 5. Total electronic linewidth and contribution to the linewidth from LO and TO phonons only. The predominant contribution of the latter phonons to the linewidth is due to the strong coupling of electrons with these phonons.

The electronic band structure, derived by solving the non-orthogonal tight-binding wave equation along the high-symmetry directions ΓKMK′Γ and ΓMΓ, is shown in figures 3(a) and 3(b). In the vicinity of the Fermi energy, chosen to be zero, only the conduction π* band and valence π band, arising from the p_z orbitals (the *z* axis is perpenducular to the plane of graphene) are present. An amazing feature of the band structure is the linear dispersion of the two bands close to the Fermi energy at the K and K′ points. The linear bands form cones above and below the zero-energy **k**-vector plane, so-called *Dirac cones*. In the effective-mass approximation, the effective-mass wave equation has the form of the wave equation of Dirac – Weil for massless fermions, which is often used in the simplified description of transport and optical phenomena in graphene.

Away from the Fermi energy, there is a deviation from the linear behaviour of the bands, known as the band *warping effect*. At energies ±2.5 eV, the bands are strongly modified between the K and K′ points and have inflexion points at the M point. The behaviour of the bands around the inflexion points is especially important for this study because of the crossover behaviour of the electronic scattering mechanism upon crossing these points and because of the enhancement of the Raman intensity in the vicinity of these points due to the logarithmic singularity of the electronic density of states (DOS) [15] (figure 3(c)).

The phonon dispersion is obtained from the dynamical equation for graphene (figure 4). The phonon branches are marked by symbols, characterizing their vibrational pattern. The longitudinal, transverse, and out-of-plane branches are denoted by the letters “L”, “T”, and “Z”, respectively. A second letter “A” and “O” is added to the branch notation with the meaning of acoustic and optical, respectively. While all branches give contribution to the two-phonon bands, here we are particularly concerned with the LO and TO branches, from which the most intense Raman lines arise.

Finally, the energy dependence of the electronic linewidth is calculated by considering all electron-phonon scattering processes in the entire Brillouin zone (figure 5). As it is seen in figure 5, the LO and TO branches are most effective in scattering electrons, which is in accord with the result of the complete calculation (not provided here) that the remaining branches produce two-phonon Raman bands with relatively low intensity.

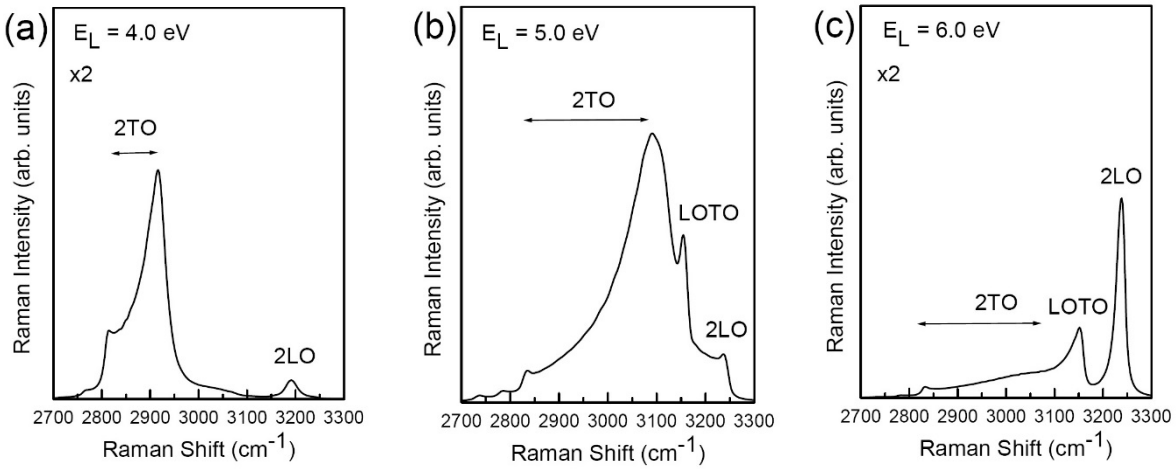

Figure 6. Calculated two-phonon Raman bands at: (a) E_L = 4.0 eV, (b) E_L = 5.0 eV, and (c) E_L = 6.0 eV.

Before proceeding with the results for the two-phonon bands, we note that the expression within the absolute value bars of equation (1) is the *scattering amplitude*. It describes *scattering processes*, consisting of virtual processes of electron-hole creation, scattering of an electron (or a hole) by a phonon, a consecutive scattering of an electron (or a hole) by a phonon with opposite momentum with regard to the first phonon, and final electron-hole annihilation. There are altogether eight different scattering processes and all of them are taken into account here. A simplified schematic of one of the eight scattering processes in graphene is displayed by a closed rectangle drawn by horizontal and vertical arrows in figure 3(a). The vertical arrows depict electron-hole creation or annihilation. For resonant processes, the vertical lines roughly correspond to the laser excitation. The horizontal arrows depict the phonon wavevectors for electron-phonon scattering processes I, II, III, and IV (figures 3(a) and 3(b)).

The calculated two-phonon Raman spectrum at E_L = 4.0 eV and in the frequency range between 2700 and 3300 cm^{-1} is shown in figure 6(a) and the participating phonons are marked by circles in figure 4. The intense band between 2800 and 2900 cm^{-1} comes from scattering by TO phonons close to the K point and is referred to as the 2TO band or the 2D band. The major contribution to this band (right peak) is due to processes I, while a minor contribution (left kink) is due to processes II. The asymmetry of this band can be attributed to the asymmetry of the TO branch with respect to the K point. The weak band at 3200 cm^{-1} arises from processes III triggered by LO phonons close to the Γ point and is known as the 2LO band.

With increasing E_L beyond the π-plasmon energy, process I disappears and a new process IV becomes effective. Recently, similar crossover behaviour has been predicted for the isostructural material silicene [16].

The two-phonon Raman spectrum at E_L = 5.0 eV, shown in figure 6(b), exhibits a broad Raman feature between 2800 and 3050 cm^{-1}, which is the 2TO band. The peak at 3050 cm^{-1} originates from processes I involving TO phonons close the Γ point and the kink at 2800 cm^{-1} originates from processes II with TO phonons close to the K point. The high-frequency kink at about 3250 cm^{-1} comes from processes III involving LO phonons close to the maximum (“overbending”) of the LO branch (2LO band). At this laser excitation, a new scattering process IV appears (see figure 3(b)). The sharp line at 3150 cm^{-1} is due to processes IV with participation of LO and TO phonons close to the Γ point (a combination LOTO band). The overall shape of the Raman bands corresponds very well to the experimentally observed one [10], which supports the applicability of the applied computational approach to the calculation of the two-phonon bands of graphene.

The two-phonon Raman spectrum at E_L = 6.0 eV shows a broad band and two sharp bands arising from processes IV with LO and TO phonons in the vicinity of the Γ point. The former is the 2TO band, and the latter are the combination LOTO band and the 2LO band.

We note that the position of the 2TO, 2LO, and LOTO bands depends on the laser excitation, which is most strongly expressed in the case of the 2TO band. The reason for this dependence is that the condition for resonance interconnects the wavevectors of the electron and the phonon, as well as the difference of the energy of the electron and hole, the phonon energy, and the laser excitation. The derived average slope of this dependence (termed *dispersion rate*) for the 2TO band of 150 cm^{-1}/eV in the energy range 2.0 – 5.0 eV agrees well with the experimental one of 165 cm^{-1}/eV [10].

Finally, the enhancement of the Raman intensity close to the π-plasmon energy of about 5 eV (figure 6(b)) can be attributed to the singularities of the electronic DOS at the M point (see also Ref. [16]).

4. Conclusions

We have shown that the position of the two-phonon Raman bands can be associated with phonons inside the Brillouin zone. These predictions can be used for reconstruction of the phonon dispersion of graphene on the basis of experimental two-phonon Raman data.

Acknowledgments

The author would like to acknowledge the financial support from EU Seventh Framework Programme project INERA under grant agreement number 316309.

References

[1] Geim A K and Novoselov K S 2007 *Nature Materials* **6** 183
[2] Castro Neto A H, Guinea F, Peres N M R, Novoselov K S and Geim A K 2009 *Rev. Mod. Phys*. **81** 109
[3] McCann E and Koshino M 2013 *Rep. Prog. Phys*. **76** 056503
[4] Bonaccorso F, Sun Z, Hasan T and Ferrari A C 2010 *Nature Photonics* **4** 611
[5] Malard L M, Pimenta M A, Dresselhaus G and Dresselhaus M S 2009 *Phys. Rep*. **473** 51
[6] Ferrari A C and Basko D M 2013 *Nature Nanotechnology* **8** 235
[7] Thomsen C and Reich S 2000 *Phys. Rev. Lett*. 85 5214
[8] Venezuela P, Lazzeri M and Mauri F 2011 *Phys. Rev*. B **84** 035433
[9] Popov V N and Lambin Ph 2012 *Eur. Phys. J*. B **85** 418
[10] Tyborski C, Herziger F, Gillen R and Maultzsch J 2015 *Phys. Rev*. B **92** 041401(R)
[11] Popov V N and Henrard L 2004 *Phys. Rev*. B **70** 115407
[12] Porezag D, Frauenheim T, Köhler T, Seifert G and Kaschner R 1995 *Phys. Rev*. B **51** 12947
[13] Popov V N and Lambin Ph 2006 *Phys. Rev*. B **73** 085407
[14] Popov V N, Henrard L and Lambin Ph 2005 *Phys. Rev*. **72** 035436
[15] Hove L V 1953 *Phys. Rev*. **89** 1189
[16] Popov V N and Lambin Ph 2016 *2D Materials* **3** 025014